Development of a Robust and Cost-Effective Friction Stir Welding Process for Use in Advanced Military Vehicles

M. Grujicic, G. Arakere, B. Pandurangan, A. Hariharan, C.-F. Yen, and B.A. Cheeseman

(Submitted February 5, 2010)

To respond to the advent of more lethal threats, recently designed aluminum-armor-based military-vehicle systems have resorted to an increasing use of higher strength aluminum alloys (with superior ballistic resistance against armor piercing (AP) threats and with high vehicle-light weighing potential). Unfortunately, these alloys are not very amenable to conventional fusion-based welding technologies and in-order to obtain high-quality welds, solid-state joining technologies such as Friction stir welding (FSW) have to be employed. However, since FSW is a relatively new and fairly complex joining technology, its introduction into advanced military vehicle structures is not straight forward and entails a comprehensive multi-step approach. One such (three-step) approach is developed in the present work. Within the first step, experimental and computational techniques are utilized to determine the optimal tool design and the optimal FSW process parameters which result in maximal productivity of the joining process and the highest quality of the weld. Within the second step, techniques are developed for the identification and qualification of the optimal weld joint designs in different sections of a prototypical military vehicle structure. In the third step, problems associated with the fabrication of a sub-scale military vehicle test structure and the blast survivability of the structure are assessed. The results obtained and the lessons learned are used to judge the potential of the current approach in shortening the development time and in enhancing reliability and blast survivability of military vehicle structures.

---

1. Introduction

Friction stir welding (FSW) is a solid-state metal-joining process that was invented in 1991 at The Welding Institute in the United Kingdom (Ref 1). FSW can be used to produce butt, corner, lap, T, spot, fillet, and hem joints, as well as to weld hollow objects, such as tanks and tubes/pipes, stock with different thicknesses, tapered sections and parts with three-dimensional contours. This welding process is particularly suited for butt and lap joining of aluminum alloys which are otherwise quite difficult to join using conventional arc/fusion welding processes. FSW has established itself as a preferred joining technique for aluminum components and its applications for joining other *difficult-to-weld* metals are gradually expanding. Currently, this joining process is being widely used in many industrial sectors such as shipbuilding and marine, aerospace, railway, land transportation, etc.

The basic concept behind FSW is described using the example of butt welding, Fig. 1. As shown in Fig. 1, a non-consumable rotating tool moves along the contacting surfaces of two rigidly butt-clamped plates. As seen in this figure, the tool consists of a cylindrical pin which is threaded, at one end, and equipped with a shoulder, at the other. Also, during joining, the work-piece (i.e., the two clamped plates) is generally placed on a rigid backing support. At the same time, the shoulder is forced to make a firm contact with the top surface of the work-piece. As the tool rotates and moves along the butting surfaces, heat is being generated at the shoulder/work-piece and, to a lesser extent, at the pin/work-piece contact surfaces, as a result of the frictional-energy dissipation. This, in turn, causes an increase in temperature and gives rise to softening of the material adjacent to these contacting surfaces. As the tool advances along the butting surfaces, thermally softened material in front of the tool is (heavily) deformed, extruded around the tool to the region behind the tool and compacted/forged to form a joint/weld.

Relative to the traditional fusion-welding technologies, FSW offers a number of advantages such as:

(a) good mechanical properties in the *as-welded* condition and substantial improvements in the consistency of weld quality (even in those alloys that are considered non-weldable by conventional techniques);

(b) improved safety due to the absence of toxic fumes or the spatter of molten material;

(c) no consumables such as the filler metal or gas shield are required;

(d) ease of process automation;

(e) ability to operate in all positions (horizontal, vertical, overhead, orbital, etc.), as there is no weld pool;

(f) minimal thickness under/over-matching which reduces the need for expensive post-weld machining;

(g) low environmental impact;

M. Grujicic, G. Arakere, B. Pandurangan, and **A. Hariharan**, Department of Mechanical Engineering, Clemson University, Clemson, SC 29634; and **C.-F. Yen** and **B.A. Cheeseman**, Army Research Laboratory, Survivability Materials Branch, Aberdeen, Proving Ground, MD 21005-5069. Contact e-mails: mica.grujicic@ces.clemson.edu and mica@ces.clemson.edu.
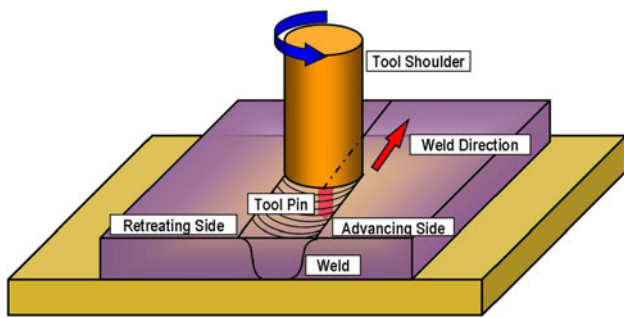
Fig. 1 A schematic of the friction stir welding (FSW) process

(h) aluminum-alloy welds in a 0.02-3.0 in range can be produced and, typically, in a single pass;

(i) dissimilar aluminum-alloy grades (e.g., AA6061 to AA5083), wrought and cast aluminum alloys, as well as aluminum matrix composites can be readily FSWed;

(j) due to lower attendant temperatures, the residual stresses and distortions are substantially reduced in comparison to those encountered in traditional arc welding processes;

(k) the innermost zone of the FSW joint typically consists of a fine equiaxed grain structure which may possess superior impact resistance properties;

(l) a complete absence of filler-induced defects (since, FSW is a filler-less process) and hydrogen-embrittlement cracking (since no hydrocarbon fuel is used);

(m) the joining process can be carried out by using modified traditional machine tool technologies;

(n) replacement of fastened joints with FSW joints can lead to significant weight reduction and cost savings;

(o) since FSW is a solid-state process, the joint is free of solidification-induced defects and, consequently, certain 2xxx and 7xxx aluminum alloys which are difficult to join using conventional fusion welding processes can be readily FSWed.

Unfortunately, the FSW technology is burdened by several disadvantages such as:

(a) an exit hole is left after the tool is withdrawn from the work-piece;

(b) relatively large tool press-down and plates-clamping forces are required;

(c) lower flexibility of the process with respect to variable-thickness and non-linear welds;

(d) often associated with lower welding rates than conventional fusion-welding techniques, although this shortcoming is somewhat lessened since fewer welding passes are required; and

(e) FSW equipment cost is typically significantly higher than the equipment cost encountered in most traditional fusion welding processes. This disadvantage is somewhat mitigated by the associated lower labor cost and by a lower need for skilled labor.

Recent efforts of the U.S. Army have been aimed at becoming more mobile, deployable, and sustainable while maintaining or surpassing the current levels of lethality and survivability. Current battlefield vehicles have reached in excess of 70 tons due to ever increasing lethality of ballistic threats which hinders their ability to be readily transported and sustained. Therefore, a number of research and development programs are under way to engineer light-weight, highly mobile, transportable, and lethal battlefield vehicles with a target weight under 20 tons. To attain these goals, significant advances are needed in the areas of light-weight structural- and armor-materials development (including aluminum-based structural/armor-grade materials).

Historically, aluminum alloy AA5083-H131 has been used in military-vehicle systems such as the M1113 and the M109, in accordance with the MIL-DTL-46027J specification (Ref 2). The main reasons for the selection of this alloy are its lighter weight, ease of joining by various welding techniques, a relatively high level of performance against fragmentation-based threats, and superior corrosion resistance.

To respond to the advent of more lethal threats, recently designed aluminum-armor-based military-vehicle systems, such as the M2 Bradley Fighting Vehicle, have relied on the use of higher strength aluminum alloys, such as AA2139 (Ref 3), AA7039 (Ref 4), AA2219 (Ref 5), and AA2519 (Ref 6). These alloys provide increased ballistic protection against armor piercing (AP) threats due to their higher dynamic strength. In addition, higher quasi-static tensile strength levels offered by these alloys are very desirable for vehicle-hull designs as they enable significant reductions in the vehicle weight. However, these alloys also show some significant shortcomings primarily due to their lower fusion-based weldability and inferior corrosion resistance in comparison to that observed in AA5083-H131. Fortunately, there are efficient remedies for these shortcomings: The low corrosion-resistance shortcomings can be, in general, overcome through the use of various coating and cladding technologies (not the subject of the present work), while the low weldability shortcomings can be addressed using FSW (the main subject of the present work). However, since FSW is a relatively new and fairly complex joining technology, its introduction into advanced military vehicle structures is not straight forward and entails a comprehensive multi-prong approach. Development of one such approach is the subject of the present work.

Within the present approach, the three main stages for the introduction of FSW process into advanced military vehicle structures are identified as:

(a) Determination of the optimal tool design and the optimal FSW process parameters which result in maximal productivity of the joining process (as measured by the tool travel speed) and the highest quality of the weld (as quantified by the weld mechanical properties and their reproducibility), for a given choice of the high-strength aluminum-alloy grades being welded. As will be shown later, at this stage the traditional experimentally based process-development efforts are complimented by an extensive program of weld-material property characterization/testing and thermal/mechanical computational analyses which can help establish correlations between the FSW process parameters and the weld microstructure/mechanical properties;

(b) Identification of the optimal weld joint design for different sections of the military vehicle structures and employment of experimental test procedures (e.g., ballistic shock test, discussed later) to qualify the welded joints; and

(c) Fabrication of a sub-scale military vehicle test structure and the employment of experimental techniques to access their blast survivability.

The organization of the paper is as follows: A detailed description of the FSW process parameters (including weld tool geometry), weld material microstructure spatial distribution and temporal evolution as well as correlations between the FSW process parameters and the weld-material microstructure/ properties are all discussed in Section 2. Details pertaining to the design and testing of FSW joints for use in military vehicle structures are presented in Section 3. A brief discussion regarding the fabrication and blast-survivability testing of the sub-scale military vehicle test structure is provided in Section 4. It should be noted that due to the sensitive nature of the subject matter and for the potential misuse of the findings obtained in the present work, some critical quantitative results had to be left out. The main conclusions resulting from the present study are summarized in Section 5.

2. FSW Process and Weld Joint Material Analysis

2.1 FSW Process

2.1.1 Mass/Heat Transport and Thermo-mechanical Aspects. FSW normally involves complex interactions and competition between various thermo-mechanical processes such as frictional-energy dissipation, plastic deformation, and the associated heat dissipation, material transport/flow, dynamic recrystallization, local cooling, etc. (Ref 7-14). A unique feature of the FSW process is that heat transfer does not only take place via thermal conduction but also via transport of the work-piece material adjacent to the tool from the region in front to the region behind the advancing tool. In general both the heat and the mass transfer depend on the work-piece material properties, tool geometry, and the FSW process parameters. As will be discussed later in greater details, mass transport is accompanied by extensive plastic deformation and dynamic recrystallization of the transported material. The attendant strain rates as high as 10 s^{-1} have been assessed/measured (Ref 15, 16).

2.1.2 Process Parameters. The main FSW process parameters which affect both the weld quality and the process efficiency are: (a) rotational and transverse velocities of the tool; (b) tool-plunge depth; (c) tool tilt-angle; and (d) tool-design/material. Since, in-general, higher temperatures are encountered in the case of higher rotational and lower transverse tool velocities, it is critical that a delicate balance between these two velocities is attained. In other words, when the temperatures are not high enough and the material has not been sufficiently softened, the weld zone may develop various flaws/defects arising from low ductility of the material. Conversely, when the temperatures are too high undesirable changes in the material microstructure/properties may take place and possibly incipient-melting flaws may be created during joining. To ensure that the necessary level of shoulder/ work-piece contact pressure is attained and that the tool fully penetrates the weld, the tool-plunge depth (defined as the depth of the lowest point of the shoulder below the surface of the welded plate) has to be set correctly. Typically, insufficient tool-plunge depths result in low-quality welds (due to inadequate forging of the material at the rear of the tool), while excessive tool-plunge depths lead to under-matching of the weld thickness compared to the base-materials thickness. Tool rearward tilting by 2-4 degrees has been often found to be beneficial since it enhances the effect of the forging process.

Tool design is one of the most important factors that influences the FSW joint profile as well as the weld material microstructure and properties. Initially, one-piece steel tools were used with both the pin and the shoulder having a (smooth-surface) right circular cylindrical geometry. Consequently, only limited material flow and mixing were produced. The two-piece FSW tools used today typically contain (flat-ended) threaded, fluted, and/or frustum (with flats) pin designs which promote material transport around the tool as well as in the work-piece through-the-thickness direction. This, in turn, enables higher weld speeds and higher quality void free weld joints. In addition, current FSW tools contain scrolled shoulders which eliminates the need for the aforementioned tool tilting (facilitate welding around corners and production of non-linear welds), weld surface undercutting and the flash that extrudes under the tool shoulder. Novel FSW tools often contain non-circular (e.g., oval, paddle, etc.) cross sections to increase the volume of stirred material and improve weld properties. Tool design is probably the most guarded secret in FSW community, as companies/researchers are generally reluctant to disclose tooling information.

2.1.3 Weld Advancing and Retreating Sides. When analyzing the FSW process, one often makes a distinction between the so-called *advancing* side of the weld (the side on which the peripheral velocity of the rotating tool coincides with the transverse velocity of the tool) and the *retreating* side (the side on which the two velocities are aligned in the opposite directions). It is generally recognized that the differences in the two weld sides give rise to asymmetry in heat transfer, material flow, and weld microstructure-properties (Ref 17).

2.2 Weld Material Microstructure/Property Distribution and Evolution

2.2.1 Weld Zones and Associated Microstructure Characteristics. Metallographic examinations of the FSW joints typically reveal the existence of the following four zones, Fig. 2:

(a) an un-effected zone which is far enough from the weld so that material microstructure/properties are not altered by the joining process;

(b) the heat-affected zone (HAZ) in which material microstructure/properties are effected only by the thermal effects associated with FSW. While this zone is normally found in the case of fusion-welds, the nature of the microstructural changes may be different in the FSW case due to generally lower temperatures and a more diffuse heat source;

(c) the thermo-mechanically affected zone (TMAZ) which is located closer than the HAZ zone to the butting
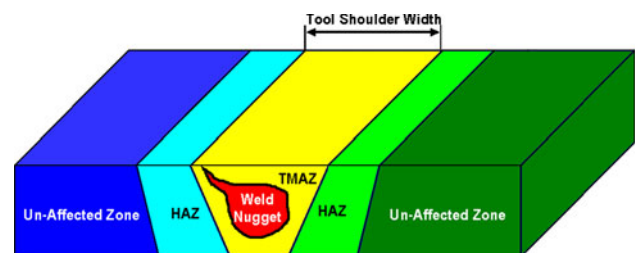

Fig. 2 A schematic of the four microstructural zones associated with the typical FSW joint

surfaces. Consequently both the thermal and the mechanical aspects of the FSW affect the material microstructure/properties in this zone. Typically, the original grains are retained in this zone although they may have undergone severe plastic deformation; and

(d) the weld *nugget* is the innermost zone of an FSW joint. As a result of the way the material is transported from the regions ahead of the tool to the wake regions behind the tool, this zone typically contains the so called "*onion-ring*" features. The material in this region has been subjected to most severe conditions of plastic deformation and high temperature exposure and consequently contains a very-fine dynamically recrystallized equiaxed grain microstructure.

2.2.2 Weld Microstructure Evolution During FSW Process. As clearly demonstrated in our prior work (Ref 18), while weld-microstructure evolution will vary with the choice of base materials and FSW process parameters, these changes show some clear differences between non-heat treatable (non age-hardenable) and heat treatable aluminum-alloy grades. Specifically, in the case of non-age-hardenable alloys (e.g., AA5083), the dominant microstructure evolution processes taking place during FSW are extensive plastic deformation and dynamic recrystallization of highly deformed material subjected to elevated temperatures approaching the solidus temperature of the alloy. On the other hand, in the case of age-hardenable alloys (e.g., AA2139), in addition to plastic deformation and dynamic recrystallization, precipitate coarsening, over-aging, dissolution, and re-precipitation typically take place.

2.2.3 Weld Microstructure/Property Relations. Taking into account the basic physical metallurgy aspects of the alloys being welded and considering the aforementioned spatial distribution and temporal evolution of the weld-material microstructure, it is to be expected that local material properties (in particular mechanical properties) may vary over the weld joint.

In the case of non-heat treatable aluminum alloys material strength (and ductility) is controlled by the following strengthening mechanisms:

(a) *Solid Solution Strengthening*: This hardening mechanism is present in all four weld-zones and its contribution to the material hardness is expected to be fairly uniform across the entire weld region;

(b) *Strain Hardening*: When a non-heat treatable alloy is cold worked, strain hardening mechanism provides a contribution to the material hardness in the base-metal zone which is larger than the contributions of the other two mechanisms. In the HAZ, some annealing will take place. However, since this annealing is primarily due to recovery or polygonization, the contribution of strain hardening to the material hardness in this region will remain quite comparable to that in the base metal region. The contribution of strain hardening to the overall material hardness in the TMAZ is expected to increase since the material in this region typically experiences significant levels of plastic deformation. In the weld nugget region, material microstructure and properties are dominated by dynamic recrystallization and, hence, the contribution of strain hardening to the overall material hardness in this region is minimal; and

(c) *Grain Size Refinement*: Since, to a first-order approximation, the average grain size does not change between the base-metal zone, the HAZ and the TMAZ, the contribution of this strengthening mechanism to the overall material strength is expected to be comparable in these three weld-zones. On the other hand, dynamic recrystallization yields a very fine grain structure within the nugget zone so that the overall contribution of the grain-refinement mechanism to the material hardness is expected to be largest in this weld zone.

In the case of heat treatable aluminum alloys material strength (and ductility) is controlled by the following strengthening mechanisms: (a) precipitation hardening; (b) strain hardening; and (c) grain-size refinement. Relative importance of the strain hardening and the grain-size refinement mechanisms within the four weld-zones was discussed earlier in the context of non-heat treatable alloys. The main points made at that time are equally valid in the case of heat-treatable alloys. As far as the role of the precipitation hardening mechanism in heat-treatable alloys is concerned, the following main observations can be made. Typically in heat-treatable alloys, precipitation hardening provides a contribution to the material hardness in the base-metal zone which is larger than the contributions of the other two mechanisms. In general, material exposure to high-temperatures within the remaining three main weld-zones causes over-aging and the associated loss in material strength. This loss increases in its extent as one approaches the original weld-line, i.e., as one moves through the HAZ, then through the TMAZ and ultimately through the weld nugget.

2.3 Correlation Between FSW-Process Parameters and Weld Joint Material Performance

2.3.1 Experimental Approach. Over the last two decades, considerable experimental research efforts have been invested toward providing a better understanding of the FSW joining mechanism and the accompanying evolution of the welded-materials microstructure/properties (e.g. Ref 19-22) as well as to rationalizing the effect of various FSW process parameters on the weld quality/integrity (e.g. Ref 10, 23-25). It should be recognized, however, that the aforementioned experimental efforts were able to only correlate the *post-mortem* welded-materials microstructure/properties with the FSW process parameters and provided relatively little real-time insight into the physics of heat/mass transfer and microstructure-evolution processes. As shown in our previous work (Ref 26), this insight can be gained by carrying out a detailed physically based computational analysis of the FSW process. Nevertheless, experimental techniques involving weld-material microstructure and property characterizations for FSW joints obtained under various combinations of process parameters and the tool geometry remain invaluable for calibration and validation of the aforementioned computational-based analyses. The weld material microstructure characterization techniques typically include optical, scanning-electron and transmission-electron microscopies, and x-ray diffraction analysis. Among the weld-material mechanical property characterization techniques the most widely used are transverse tensile tests, all-weld longitudinal tensile test and a transverse bend test (Ref 27).

2.3.2 Computational Approach. A detailed review of the prior research efforts dealing with computational investigations of the FSW process reported in the public domain

literature was conducted in our previous work (Ref 26). Hence, no overview of the prior computational FSW research efforts will be presented here. Instead, a brief overview will be provided of our recent fully coupled thermo-mechanical finite-element analysis of the FSW process which combines the mass, momentum, and heat-transfer conservation equations with the basic physical metallurgy (microstructure evolution) of the aluminum alloy grades being FSWed (Ref 26). Within this analysis, various microstructure-evolution processes taking place during FSW (e.g., extensive plastic-deformation induced grain-shape distortion and dislocation-density increase, dynamic recrystallization, and precipitates coarsening, over-aging, dissolution, and re-precipitation) are considered to predict the material microstructure/properties in the various FSW zones of the alloys being welded. For each of the aforementioned microstructure evolution processes, the appropriate material state variables are introduced and their evolution equations constructed and parameterized (using available open literature sources pertaining to the kinetics of the microstructure evolution processes). Next, the thermo-mechanical constitutive model for the alloys being FSWed is modified to include the effect of the local material microstructure. This procedure enabled examination of the two-way interactions between the FSW process and the weld-material microstructure evolution. In other words, both the effect of the current material microstructure on its thermo-mechanical response during the FSW process and the effects of thermo-mechanical history of a material point during the FSW process on the associated microstructure could be analyzed.

In the remainder of this section a few typical FSW process simulation results obtained using our FSW model (Ref 26) are presented and briefly discussed.

Equivalent Plastic Strain Field. An example of the typical results pertaining to spatial distribution and temporal evolution of the equivalent plastic strain in the work-piece during FSW is displayed in Fig. 3(a-d). Simple examination of the results like the ones displayed in these figures but generated under different FSW process conditions reveals that: (a) depending on the FSW process conditions such as tool contact pressure, tool rotational and translational speeds, equivalent plastic strains in a range between 20 and 50 are observed; (b) the highest equivalent plastic strains are always found in the work-piece material right below the tool shoulder and equivalent plastic strains progressively decreased from this region as a function of the distance in the radial and through-the-thickness directions; (c) there is a highly pronounced asymmetry in the distribution of the equivalent plastic strain relative to the initial location of the butting surfaces. This asymmetry is related to the aforementioned differences in the material transport (at the advancing and the retreating sides of the weld) from the region ahead of the tool to the region behind the tool; and (d) as the tool translational speed is decreased and the tool/work-piece contact pressure is increased, higher equivalent plastic strains are observed and equivalent plastic strain differences between the top and bottom surfaces of the work piece are reduced. This finding suggests that under these FSW process conditions the extent of material stirring/mixing (which plays a critical role in weld quality/joint-strength) is increased.

Nodal Velocity Field. The distribution of nodal velocities at the outer surfaces of the work-piece at two different times (0.0 and 0.5 s) is displayed in Fig. 4(a-b). For clarity, the tool is not shown. These figures clearly show that the initially assigned unidirectional velocity field (to the work-piece material within the Arbitrary-Lagrangian-Eulerian (ALE) finite-element formulation used in Ref 26) in the direction of welding, quickly transforms into the velocity field in which there is a well-defined stir region right below the shoulder (within which the material circles around the pin) and the remainder of the field (within which the material tends to flow around the stir region). A comparison of the results displayed in Fig. 4(a-b) clearly shows how the region underneath the tool shoulder which is initially unfilled becomes filled as FSW proceeds (please note an increase in the work-piece hole upper-rim altitude). Once the space under the shoulder is fully filled it remains filled as the FSW process continues. The material in this region is constantly being refreshed as the tool advances in the welding direction.
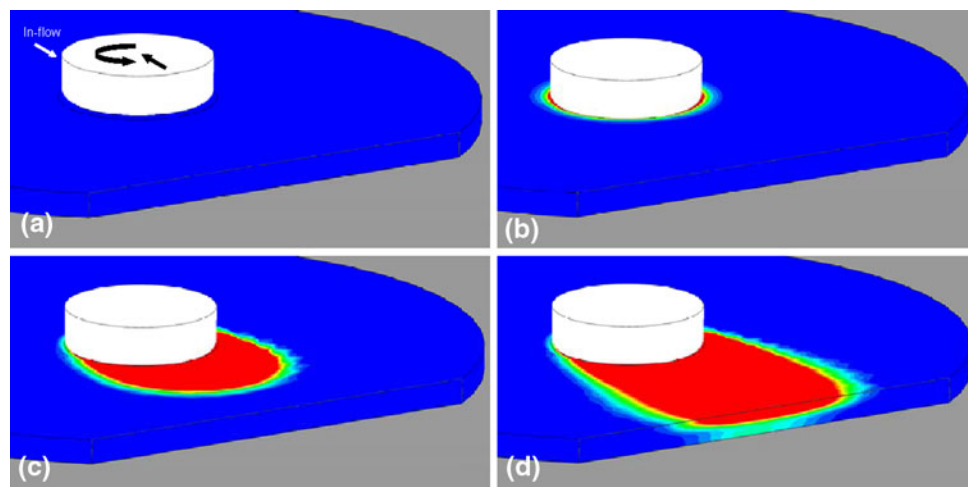

Fig. 3 Typical results pertaining to spatial distribution and temporal evolution of the equivalent plastic strain during FSW: (a) zero-time step; (b) at the end of tool-insertion; (c) 7 s afterwards; and (d) 14 s afterwards. Equivalent-plastic strain range: 0.0 (*blue*) to 50.0 (*red*)
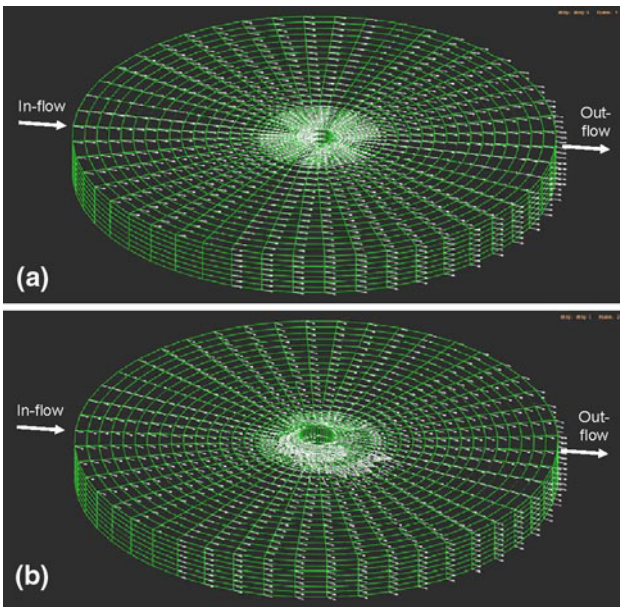
Fig. 4 A typical nodal-velocity field associated with friction stir welding: (a) the initial state; (b) the fully developed state

Fig. 5 (a) Retreating-side and (b) advancing-side tracer-particle typical trajectories

Material/Tracer Particle Trajectories. The results displayed in Fig. 4(a-b) show the spatial distribution and temporal evolution of the nodal velocities. It should be noted that due to the ALE character of the finite-element analysis used in Ref 26, the motion of the finite-element mesh is not completely tied to the motion of the material. Thus, the results displayed in Fig. 4(a-b) show the velocities of the material particles which at that moment pass through the nodal points in question. However, at different times different material particles are associated with the same nodes. To observe material extrusion around the tool pin and its forging at the tool wake, it is more appropriate to construct and analyze material-particle trajectories. This was made possible within ABAQUS/Explicit finite element code employed in Ref 26 through the use of so-called "*tracer particles*" which are attached to the material points (and not to the mesh nodal points).

An example of the prototypical results pertaining to the trajectory of retreating-side and advancing-side tracer particles is displayed in Fig. 5(a-b), respectively. The tracer particles displayed in these figures are initially located in a plane which is halfway between the top and bottom surfaces of the work-piece. For improved clarity, tracer-particle trajectories are color coded. The results displayed in Fig. 5(a-b) clearly revealed the following basic aspects of the FSW process: (a) the work-piece material at the retreating side (as represented by the yellow and green tracer-particle trajectories, Fig. 5a), does not, for the most part, enter the stir zone under the tool-shoulder and usually only flows around it; (b) the material at the advancing side (as represented by the white and cyan tracer-particle trajectories, Fig. 5b), which is initially close to the butting surfaces, passes over to the retreating side and is co-stirred with some of the retreating-side material to form the welded joint; and (c) the advancing-side material further away from the initial butting surfaces remains on the advancing side and either enters the stir region on the advancing side or flows around it.
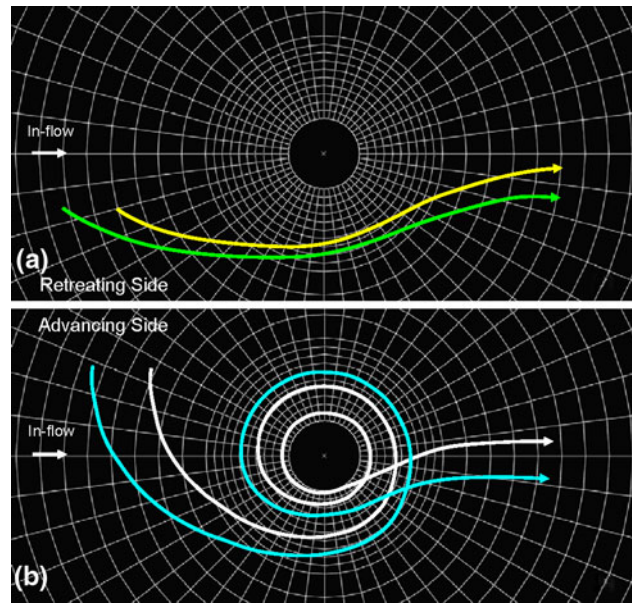
Material Hardness Field. Variation of the material hardness measured transversely across the friction stir weld over the top surface of the work-piece consisting of solution-strengthened and strain-hardened AA5083-H131 plates on both sides of the joint is displayed in Fig. 6(a-b). The results displayed in these two figures correspond to two different welding tool traverse speeds: (a) Figure 6(a) 100 mm/min; and (b) Fig. 6(b), 150 mm/min, while the tool rotation speed, shoulder diameter, and threaded pin diameter are kept constant at 350 rpm, 18 and 5 mm, respectively.

For comparison, the corresponding experimental results obtained in Ref 28 are also displayed in Fig. 6(a-b). Since the original hardness results reported in Ref 28 were given using Vickers hardness units, they were converted using the known indentation loads and indentor geometry data to the SI stress units before including in these figures.

Simple examination of the results displayed in Fig. 6(a-b) shows that:

(a) The computational model developed in Ref 26 yields a physically realistic variation in material hardness across the FSW joints, i.e., the computed hardness profiles clearly delineate the four different weld zones;

(b) As far as the quantitative agreement between the computed results and their counterparts from Peel et al. (Ref 28) is concerned, it can be characterized as being good to fair. Possible reasons for the observed discrepancies include: (i) deficiencies in the functional relations used to describe the contribution of various mechanisms to material hardness; (ii) diversity and scarcity of the relevant experimental data used for model parameterization; and (iii) potential inaccuracies associated with hardness measurements in Ref 28.

A comparison of the computed results (pertaining to the hardness variation in a direction transverse to the original weld
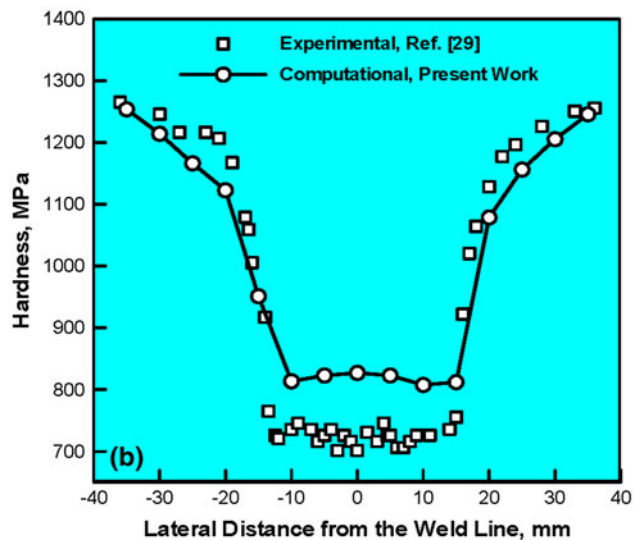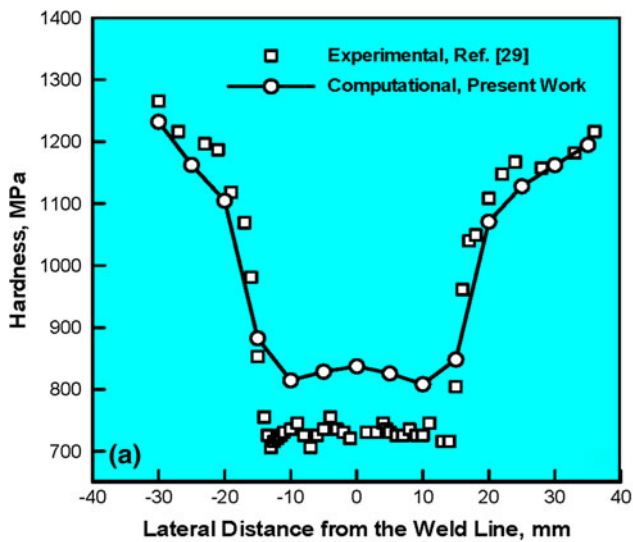
Fig. 6 A comparison between the computed and the experimental hardness (transverse) profiles over the top surface of the 5083 work piece. Please see the text for details regarding the friction stir weld parameters associated with the results displayed in (a) and (b). Data pertaining to the advancing side of the weld joint are on the right-hand side of the plot
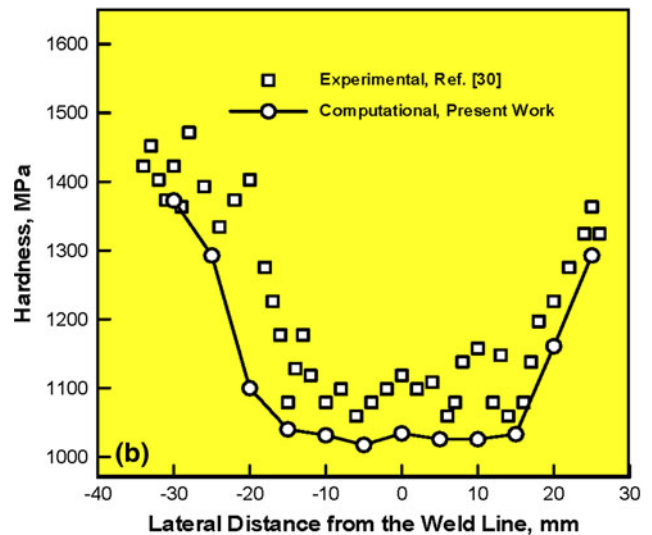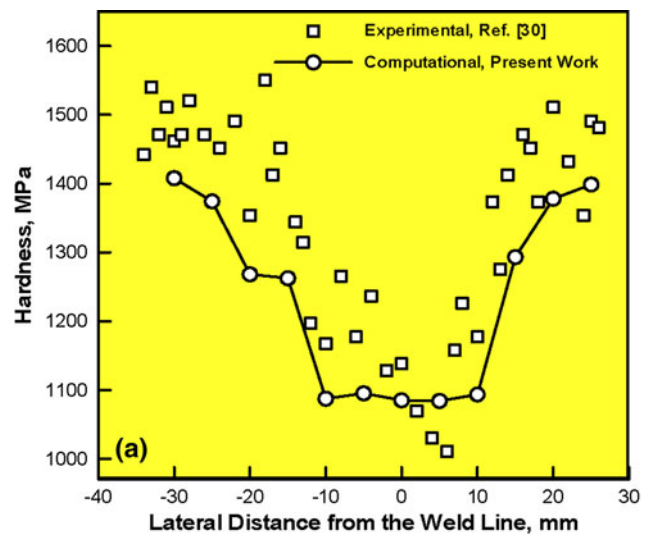
Fig. 7 A comparison between the computed and experimental hardness profiles over a transverse cut through the 2139 work piece weld: (a) top surface of the work piece and (b) the bottom surface of the work piece. Please see the text for details regarding the friction stir welding parameters. Data pertaining to the advancing side of the weld joint are on the right-hand side of the plot

line) and their experimental counterparts obtained in Ref 29 in the case of two friction-stir-welded age-hardened AA2139 plates is displayed in Fig. 7(a-b). The results displayed in Fig. 7(a-b) correspond, respectively, to the hardness measurements over the top and bottom surfaces of the work piece. In both cases the same FSW process parameters (welding speed: 100 mm/min; tool rotational speed: 350 rpm; shoulder diameter: 18 mm; and pin diameter: 5 mm) were used.

Simple examination of the results displayed in Fig. 7(a-b) shows that as in the case of AA5083, the computational model developed in Ref 26 provides physically realistic hardness profiles in a direction transversely oriented with respect to the weld (at different locations through the thickness of the work-piece).

Material Grain-Size Field. A comparison between the grain-size results obtained computationally in Ref 26 and their

experimental counterparts reported in Ref 30 is displayed in Fig. 8. Considering the fact that not all the FSW process parameters were specified in Ref 30, the level of agreement observed in Fig. 8 can be judged as reasonable.

A comparison of the computed variation in the average grain-size across the FSW joint (Ref 26) and its experimental counterpart obtained in Ref 31 is displayed in Fig. 9. These results pertain to the top surface of the work-piece. Simple examination of the results displayed in Fig. 9 shows that the computation/experiment agreement is comparable to that obtained in the case of AA5083 (i.e., the agreement is reasonable).

Residual Stress Field. A comparison between the computed (Ref 26) and the experimentally measured (Ref 28) results pertaining to variation of the longitudinal and transverse residual stresses as a function of the distance from the initial
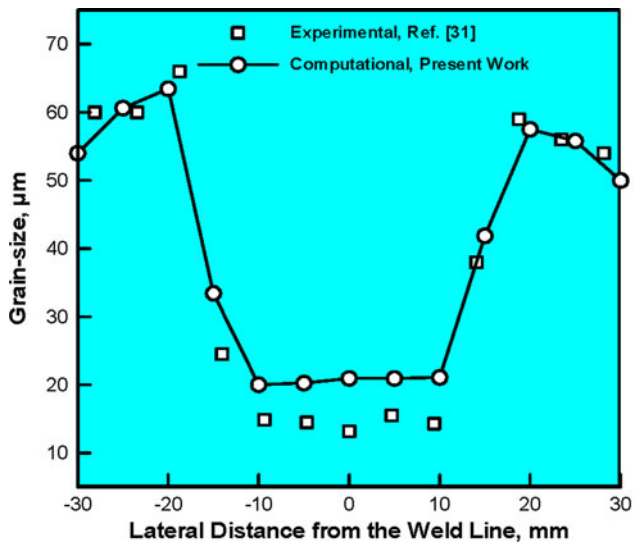
Fig. 8 A comparison between the computed and experimental grain-size profiles over the top surface of the 5083 work piece. Data pertaining to the advancing side of the weld joint are on the right-hand side of the plot
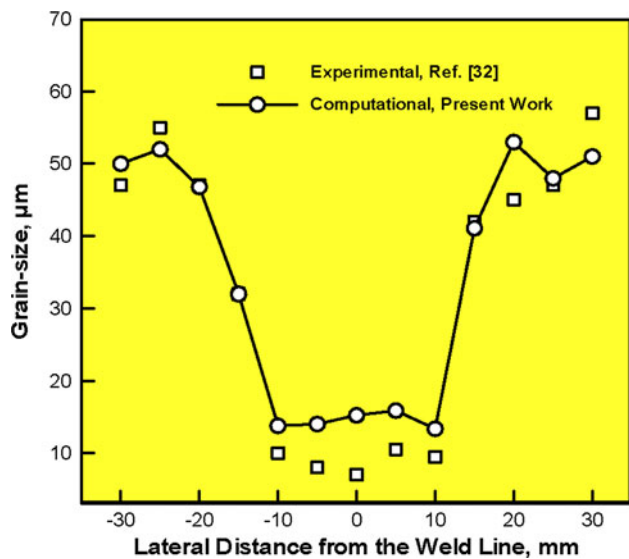

Fig. 9 A comparison between the computed and experimental grain-size profiles over the top surface of the 2139 work piece. Data pertaining to the advancing side of the weld joint are on the right-hand side of the plot

Fig. 10 Variation of the: (a) longitudinal and (b) transverse residual stresses as a function of the distance from the weld-line in 5083. Data pertaining to the advancing side of the weld joint are on the right-hand side of the plot

location of the butting surfaces in AA5083 is displayed in Fig. 10(a-b). Two sets of computational results are presented: one based on the use of the original Johnson-Cook material model while the other was based on the use of the modified Johnson-Cook model (Ref 26). Simple examination of the results presented in Fig. 10(a-b) shows that the results based on the modified Johnson-Cook model are in better agreement with the experimental results. While some disagreement still exists between the computational results based on the modified Johnson-Cook model and the experimental results, the overall residual stress distribution profile appears to be reasonably
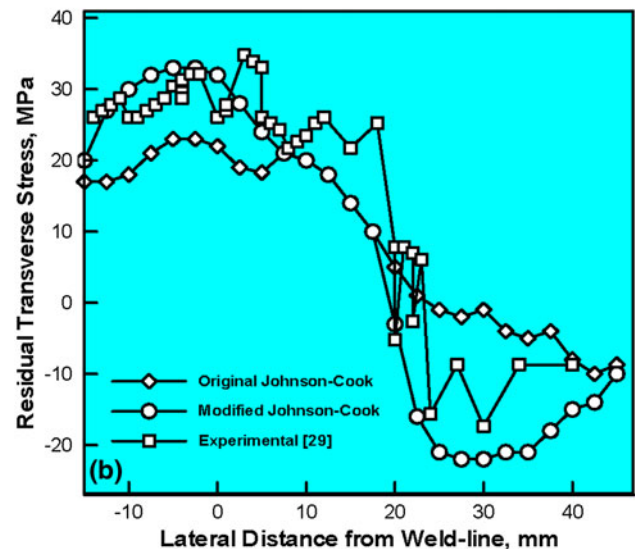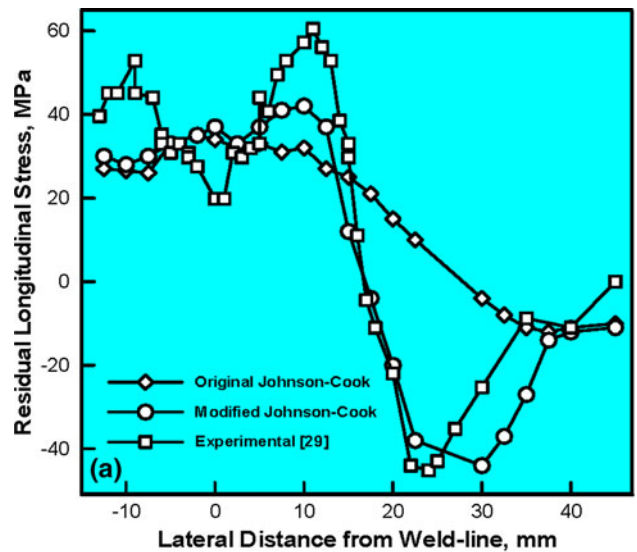
well reproduced by the computational analysis (Ref 26). Specifically:

(a) The residual stresses are compressive at larger distances from the weld-line at the advancing side of the weld (the right-hand side in Fig. 10a-b);

(b) As one approaches the weld-line at the advancing side, the residual stresses first increase in magnitude and then switch their character (i.e., becomes tensile), at a distance of 15-20 mm from the weld-line (at the advancing side);

(c) In the innermost portion of the nugget, the tensile residual stresses tend to decrease somewhat;

(d) As the distance from the weld-line increases on the retreating side, the stresses gradually decrease toward zero; and

(e) The longitudinal residual stresses are generally higher than their transverse counterparts.

2.4 FSW Process and Weld Tool Optimization

When coupled with conventional Design of Experiments (DOE) and/or Design Optimization (DO) techniques, the experimental and computational analyses overviewed in the previous section can be used to identify an optimal combination of the FSW process parameters and tool design geometrical/material parameters for a given choice of the aluminum-alloy grades and plate thicknesses. While attempting to identify optimal FSW process and weld-tool parameters, the emphasis is placed on maximizing the manufacturing efficiency of the joining process (as quantified by the tool travel speed), maximizing the quality of the FSW joint (as quantified by the material mechanical properties and their consistency) and minimizing the forces which must be applied to the tool and the work piece during the welding process (primarily the axial tool-driving and the transverse work-piece clamping forces).

2.4.1 FSW Process Optimization. The optimal FSW process parameters (for a given tool design and the choice of the aluminum-alloy grades and plate thicknesses), are generally determined by employing the computational analyses like the one reported in Ref 26. An example output from such analyses is displayed in Fig. 11 in which a thermal foot-print at the front and rear of the shoulder of the weld tool are shown. Temperature distribution within the foot-print and the knowledge of the material solidus temperature (the lowest temperature at which melting is observed) and the effect of temperature on the material strength are used to determine the optimal FSW process parameters.

This procedure typically reveals that (for a given tool design, the rotational speed of the tool and the choice of the aluminum alloy grades and plate thicknesses), there is an optimal range of the tool traverse speeds. Tool travel speeds exceeding this range typically give rise to the formation of low-ductility fl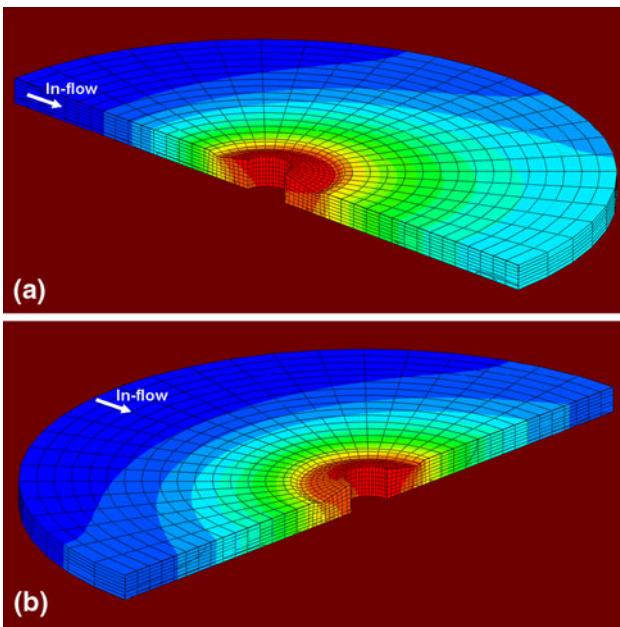aws within the weld, while, for tool speeds below this range, microstructural defects associated with excessive heating are often observed. Within this range lower velocities typically cause HAZ to possess over-aging induced inferior microstructure/properties (i.e., welds typically fracture in this weld zone). On the other hand, in the upper region of the optimal tool-speed range, failure typically occurs within the weld nugget region (since, material over-aging within the HAZ is less pronounced and the properties less degraded).

2.4.2 FSW Tool-Design Optimization. The problem of finding the optimal design of the weld tool is generally quite challenging since the tool geometry can be quite complex and entails a large number of parameters for its full description. Typically, there is an optimal pin length an optimal pin-diameter to pin-length ratio as well as an optimal pin-diameter to shoulder-diameter ratio. In addition to these tool design parameters, there is a relatively large number of parameters which describe the pin shape (i.e., thread, flute, frustum with flats, etc.), and the shoulder shape (scroll, spiral etc.).

Typically, when high strength aluminum alloys are FSWed, the optimal weld-tool design involves a flat ended threaded, frustum-shaped pin profile with three-four equally spaced flats machined into the profiled surfaces and a scroll or spiral shoulder profile, Fig. 12. The flat end of the pin helps to produce a better stir zone or weld nugget penetration to the back of the work-piece. The threaded portion of the pin body promotes material transport in the work-piece through-the-thickness direction while the frustum-shaped pin profile promotes material extrusion around the tool and its forging in the region behind the tool. The scroll shoulder design enables welding without tilting the welding tool relative to the work-piece, which facilitates welding around corners.

3. FSW Weld Joint Design and Testing

3.1 Design Considerations for the FSW Joints

3.1.1 90° Corner Joints. Construction of complex structural components such as military-vehicle underbodies/hulls typically involves not only in-plane (planar) but also out-of-plane (e.g., corner) joint configurations. Hence, one of the challenges associated with the construction of these structures
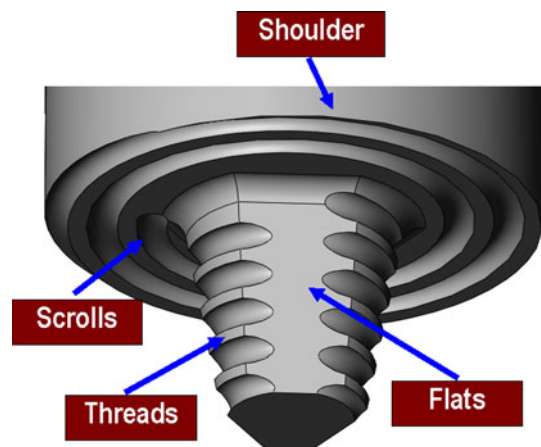
Fig. 11 Typical temperature distribution over one-half of the work-piece obtained by cutting along: (a) the longitudinal; and (b) transverse directions: Maximum (*red*) = 400 °C; Minimum (*blue*) = 25 °C

Fig. 12 Typical optimal design of the FSW tool used for joining high-strength aluminum-alloy grades

is determination of the optimal weld joint configuration(s). For example, in the case of corner FSW joints, like the one associated with the joining of the vehicle floor section to the frame sidewalls, one can choose between a butted corner joint, Fig. 13(a), and a rabbeted corner joint, Fig. 13(b). Furthermore, in the latter case, the joint is characterized by a single geometrical design parameter (the rabbet depth), Fig. 13(b).

Each of the two aforementioned corner joints possess certain advantages and shortcomings, e.g., while the butted corner joint requires less pre-weld preparation (i.e., less or no machining is required for preparation of the weld surfaces), it entails special tooling in-order to support the horizontal weld plate, Fig. 13(a). On the other hand, in the case of the rabbet corner weld joint which is commonly used in conventional arc welding, fixturing is less challenging but a segment between the horizontal and vertical members is left un-welded, Fig. 13(b). To obtain load transfer between the horizontal and vertical members in this region, it is a common arc welding practice to deposit a fillet weld along the inner edge. As shown in Fig. 14, FSW also enables formation of a seam weld along the inner edge.
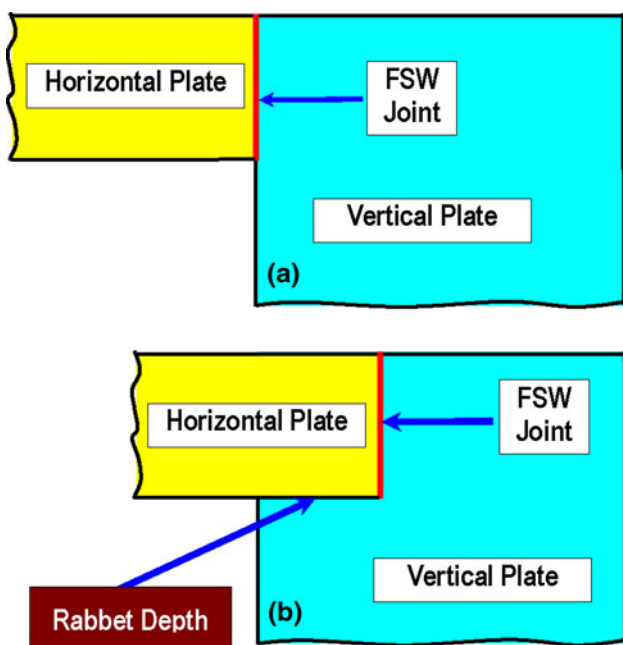
To identify the optimal FSW corner-joint configuration, it is a common practice to fabricate and test these joints. While, the mechanical response of these joints when subjected to a variety of loading conditions can be, in principle, assessed computationally, these types of computational analyses are not frequently employed. Instead, the welds are qualified almost exclusively using experimental means (e.g., the so called ballistic shock test described in the next section).

3.1.2 Low Angle Out-of-Plane Joints. Military-vehicle underbody/hull constructions often involve low angle out-of-plane joints (e.g., V-shaped hulls). While, it is, in principle, possible to produce such joints by directly welding the angled plates, the welding process is quite challenging and the weld quality is often deficient. Consequently, it is suggested that machined or extruded angular transition members be used in this case and that a single low-angle out-of-plane joint be replaced by two planar butt joints, Fig. 15(a) and (b).

3.1.3 Complex Three-Dimensional Weld Joints. Due to high complexity of the military-vehicle underbody/hull constructions, FSW weld tool is often required to follow intricate three-dimensional trajectories. Under such circumstances, it is advantageous that the tool remains normal to the outer surface of the plates being welded. As mentioned earlier, this can be attained, while ensuring a high quality of the weld, by using a scrolled shoulder. Also, to prevent the relative motion of the plates being welded and to ensure good dimensional accuracy it is suggested that the sections being joined be Friction-stir tack welded prior to being FSWed.

Fig. 13 Two designs of corner joints most often in conjunction with the FSW process: (a) butted corner joint; and (b) rabetted corner joint
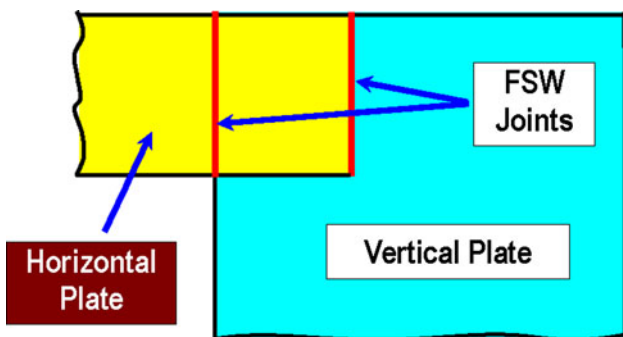

Fig. 14 Joining of the 90° angled plates along their inner edge using FSW
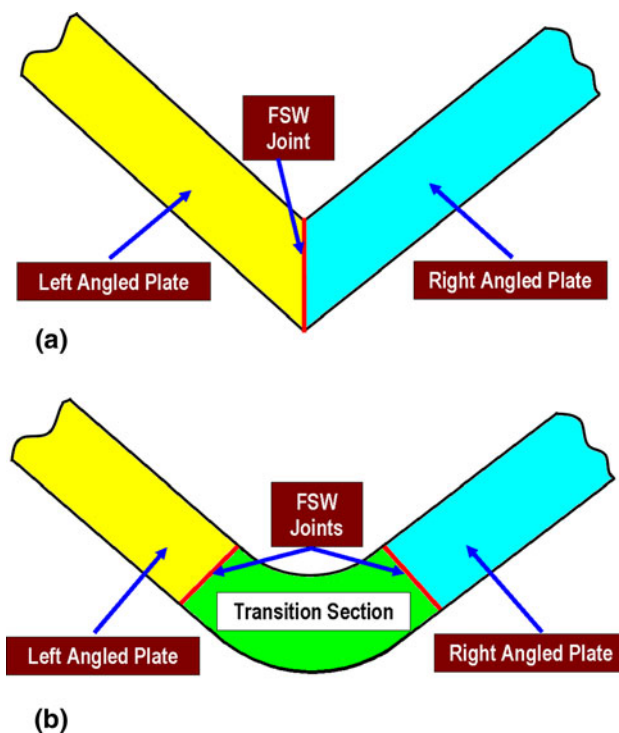

Fig. 15 Two possible designs for a low angle out-of-plane joints. A single low angle out-of-plane joint in (a) is replaced (with the help of an angular transition section) into two planar butt joints in (b)

3.2 Ballistic Shock Testing of FSW Joints

When the ability of FSW joints to withstand high-rate loading is of primary concern, these welds are typically subjected to the so called ballistic shock impact test as defined in MIL-STD-1946A (Ref 32). In accordance with this test, the weld joint is impacted by a 75 mm-diameter/150 mm-length solid right circular cylindrical aluminum slug at a velocity defined by the attendant aluminum alloy grades and plate thicknesses. For the weld to qualify, the total crack length must not exceed 305 mm.

When the ballistic shock test is used to qualify butted corner and rabetted corner FSW joints, clear differences between these two types of weld designs are often observed. That is, the butted corner joint is often found to out perform the rabetted corner joint with respect to the ballistic shock loading. This finding may have significant economical benefits since the use of the butted corner joint reduces the production costs by eliminating the need for pre-weld machining of the rabbet.

The aforementioned differences between the two corner-joint designs can be rationalized as follows: (a) In the case of the inferior rabetted-corner joint, the HAZ was often found to extend across the inner most edge of the two plates where, under dynamic loading conditions, shear stresses are the highest, Fig. 16. Since, in this case, the over-aged inferior HAZ microstructure is located in the region associated with the most severe loading, it is no surprise that rabetted corner joints possess sub-standard ballistic performance. It should be noted, however, that the actual location of the HAZ can be changed by modifying the rabbet depth which would result in an improved ballistic performance of the rabetted corner joint; and (b) In the case of the butted corner joints, fine grained weld nugget zone with superior impact strength is typically placed in the region of highest shear stresses. Since, fine grain microstructure is highly beneficial to dynamic strength of the material; the superior ballistic performance of the butted joint is justified.
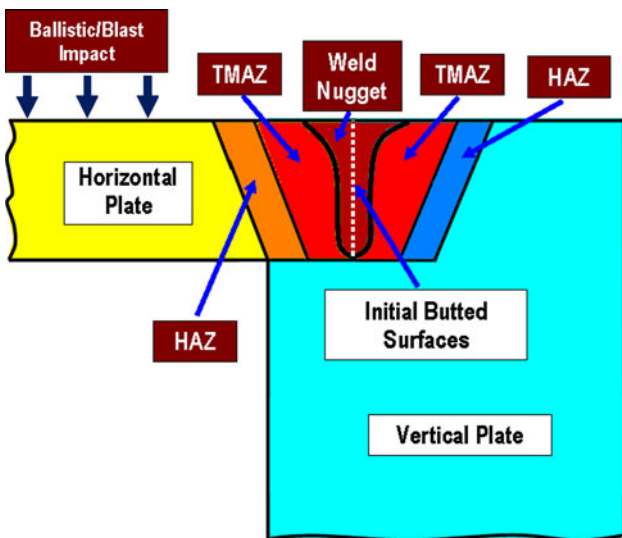

Fig. 16 A possible reason for the inferior ballistic performance of rabetted corner joints, i.e., the HAZ which contains degraded over-aged material is located in the region experiencing maximum shear stresses

4. Sub-Scale Test Structure Fabrication and Testing

Within the third stage of introduction of the FSW process in the construction of military vehicle underbodies/hulls, a sub-scale test structure is typically fabricated and tested under fairly realistic buried-mine blast loading conditions. The test structure is normally required to meet stringent conditions pertaining to the absence of penetration/fragmentation and a lack of excessive deflections. An example of the vehicle-hull test structure used in our work is displayed in Fig. 17. Due to the sensitive nature of the subject matter details regarding this test structure and its blast survivability potential could not be discussed here.

4.1 Design Consideration for the FSW Joints

When designing the test structures, it is critical to ensure that their topology and design (e.g., plates, stiffeners, and structural details) closely resemble those of prototypical military vehicles so that the results obtained can be used to judge blast survivability of the vehicle structures themselves. In addition, during fabrication of the test structures, the proper FSW practice discussed in Section 2 should be exercised in order to produce high quality flat, corner, and low-angle weld joints. Failure to do so may provide wrong/misleading information regarding the feasibility for utilizing high strength aluminum alloys and the FSW technique in manufacturing blast-survivable military-vehicle structures.

4.2 Buried-Mine Blast Testing of FSWed Military-Vehicle Test Structures

The ultimate proof for suitability of the FSW technology and high-strength aluminum alloys for use in military-vehicle underbody/hull structures is obtained during the mine-blast survivability testing stage. Within this stage, the vehicle-hull test structure is secured within a test fixture and subjected to blast loads resulting from detonation of a mine buried in soil. Since during this process a sub-scale vehicle underbody test structure is tested, the following problems must be resolved before the test results can be used to quantify blast survivability of the military vehicles in question:

(a) The manner in which the test structure is secured to the test fixture and the overall fixture weight should closely resemble their counterparts present in the vehicle.
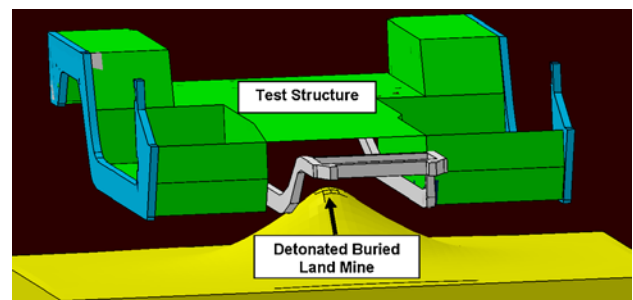

Fig. 17 An example of the sub-scale vehicle underbody/hull test structure used in mine-blast experiments in order to assess suitability of the FSW process for the fabrication of high-survivability military vehicles

This is a critical requirement since often the performance of structures (including joints) is greatly affected by the effect of surrounding constraints/interactions;

(b) If the test structure is sub-scaled then a dimensional analysis should be employed to account for the scaling effects (e.g. Ref 33);

(c) While a full-factorial blast-testing schedule over the design/test variables (mine size, shape and explosion energy, depth of burial, stand-off distance, soil type, compaction level, and degree of saturation, etc.) is preferred, in many cases blast testing under most adverse combinations of these test variables may suffice; and

(d) A comprehensive failure analysis should be conducted following each mine-blast test. Past experience has shown that one can learn a great deal about the behavior of materials and structures by investigating the manner in which they fail in the presence of various loading and constraining conditions.

5. Summary Remarks

In the present article, a procedure is developed for the introduction of friction stir welding (FSW) technology and high-strength age-hardened aluminum alloys to the construction of blast-survivable military-vehicle underbody/hull structures. The procedure involves three basic steps, Fig. 18.

Within the first step, various experimental and computational methods are employed in order to optimize the FSW process and the weld-tool design with respect to attaining high productivity of the welding process, high quality of the weld (i.e., low defect content and superior mechanical properties of the weld material) and low axial (tool driving) and transverse (work-piece clamping) forces required for the FSW process.

Within the second step, various FSW-joint designs are considered in order to identify the optimal design for different joints encountered during construction of the military-vehicle underbody/hull structures. Typical procedures used to qualify individual weld joints with respect to dynamic loads as those accompanying mine blast are also considered.

In the third step, fully fabricated (sub-scale) military-vehicle underbody/hull test structures are subjected to mine-blast loads in order to assess their level of blast survivability. The key aspects of test structures fabrication and testing as well as of the data reduction (including the scaling effects) are also discussed.

Fig. 18 A three-step procedure for the introduction of friction stir welding (FSW) technology and high-strength age-hardened aluminum alloys to the construction of blast-survivable military-vehicle underbody hull structures

References

1. W.M. Thomas, E.D. Nicholas, J.C. Needham, M.G. Murch, P. Temple-Smith, and C.J. Dawes, "Friction Stir Butt Welding," International Patent Application No. PCT/GB92/02203, 1991
2. "Armor Plate, Aluminum Alloy, Weldable 5083 and 5456," MIL-DTL-46027J, U.S. Department of Defense, Washington DC, August 1992
3. A. Cho, Alcan Rolled Products, Ravenswood, WV, USA, Private Communication, June 2009
4. "Armor Plate, Aluminum Alloy, 7039," MIL-DTL-46063H, U.S. Department of Defense, Washington DC, December 1992
5. "Aluminum Alloy Armor, 2219, Rolled Plate and Die Forged Shapes," MIL-DTL-46118E, U.S. Department of Defense, Washington DC, August 1998
6. "Aluminum Alloy Armor Rolled Plate (1/2 to 4 Inches Thick), Weldable (Alloy 2519)," MIL-DTL-46118E, U.S. Department of Defense, Washington DC, February 2000
7. H. Liu, H. Fulii, M. Maeda, and K. Nogi, Tensile Properties and Fracture Locations of Friction-Stir Welded Joints of 6061-T6 Aluminium Alloy, *J. Mater. Sci. Lett.*, 2003, **22**, p 1061–1063
8. W.B. Lee, C.Y. Lee, W.S. Chang, Y.M. Yeon, and S.B. Jung, Microstructural Investigation of Friction Stir Welded Pure Titanium, *Mater. Lett.*, 2005, **59**, p 3315–3318
9. W.M. Thomas and E.D. Nicholas, Friction Stir Welding for the Transportation Industries, *Mater. Des.*, 1997, **18**, p 269–273
10. J.Q. Su, T.W. Nelson, R. Mishra, and M. Mahoney, Microstructural Investigation of Friction Stir Welded 7050-T651 Aluminum, *Acta Mater.*, 2003, **51**, p 713–729
11. O. Frigaard, Ø. Grong, and O.T. Midling, A Process Model for Friction Stir Welding of Age Hardening Aluminum Alloys, *Metall. Mater. Trans. A*, 2001, **32**, p 1189–1200
12. M.W. Mahoney, C.G. Rhodes, J.G. Flintoff, R.A. Spurling, and W.H. Bingel, Properties of Friction-Stir-Welded 7075 T651 Aluminum, *Metall. Mater. Trans. A*, 1998, **29**, p 1955–1964
13. C.G. Rhodes, M.W. Mahoney, W.H. Bingel, R.A. Spurling, and C.C. Bampton, Effect of Friction Stir Welding on Microstructure of 7075 Aluminum, *Scripta Mater.*, 1997, **36**, p 69–75
14. G. Liu, L.E. Murr, C.S. Niou, J.C. McClure, and F.R. Vega, Microstructural Aspects of the Friction-Stir-Welding of 6061-T6 Aluminum, *Scripta Mater.*, 1997, **37**, p 355–361
15. K.V. Jata and S.L. Semiatin, Continuous Dynamic Recrystallization During Friction Stir Welding, *Scripta Mater.*, 2000, **43**, p 743–748
16. K. Masaki, Y.S. Sato, M. Maeda, and H. Kokawa, Experimental Simulation of Recrystallized Microstructure in Friction Stir Welded Al Alloy Using a Plane-Strain Compression Test, *Scripta Mater.*, 2008, **58**, p 355–360

17. J.H. Cho, D.E. Boyce, and P.R. Dawson, Modeling Strain Hardening and Texture Evolution in Friction Stir Welding of Stainless Steel, *Mater. Sci. Eng. A*, 2005, **398**, p 146–163

18. M. Grujicic, G. Arakere, H.V. Yalavarthy, T. He, C.-F. Yen, and B.A. Cheeseman, Modeling of AA5083 Material-Microstructure Evolution During Butt Friction-Stir Welding, *J. Mater. Eng. Perform.*, accepted for publication, July 2009. doi:10.1007/s11665-009-9536-1

19. W.M. Thomas, E.D. Nicholas, J.C. NeedHam, M.G. Murch, P. Templesmith, and C.J. Dawes, "Friction Stir Welding," International Patent Application No. PCT/GB92102203 and Great Britain Patent Application No. 9125978.8, 1991

20. R.S. Mishra and Z.Y. Ma, Friction Stir Welding and Processing, *Mater. Sci. Eng. R Rep.*, 2005, **50**, p 1–78

21. H.W. Zhang, Z. Zhang, and J.T. Chen, The Finite Element Simulation of the Friction Stir Welding Process, *Mater. Sci. Eng. A*, 2005, **403**, p 340–348

22. A.J. Ramirez and M.C. Juhas, Microstructural Evolution in Ti-6Al-4V Friction Stir Welds, *Mater. Sci. Forum*, 2003, **426–432**, p 2999–3004

23. H.G. Salem, A.P. Reynolds, and J.S. Lyons, Microstructure and Retention of Superplasticity of Friction Stir Welded Superplastic 2095 Sheet, *Scripta Mater.*, 2002, **46**, p 337–342

24. H.J. Liu, Y.C. Chen, and J.C. Feng, Effect of Zigzag Line on the Mechanical Properties of Friction Stir Welded Joints of an Al-Cu Alloy, *Scripta Mater.*, 2006, **55**, p 231–234

25. Z.Y. Ma, S.R. Sharma, and R.S. Mishra, Effect of Friction Stir Processing on the microstructure of Cast A356 Aluminum, *Mater. Sci. Eng. A*, 2006, **433**, p 269–278

26. M. Grujicic, T. He, G. Arakere, H.V. Yalavarthy, C.-F. Yen, and B.A. Cheeseman, Fully-Coupled Thermo-Mechanical Finite-Element Investigation of Material Evolution During Friction-Stir Welding of AA5083, *J. Eng. Manuf.*, accepted for publication, September 2009. doi:10.1243/09544054JEM1750

27. G. Campbell and T. Stotler, Friction-stir Welding of Armor Grade Aluminum Plate, *Welding J.*, 1999, **78**(12), p 4547

28. M. Peel, A. Steuwer, M. Preuss, and P.J. Withers, Microstructure, Mechanical properties and Residual Stresses as a function of Welding Speed in Aluminium AA5083 Friction Stir Welds, *Acta Mater.*, 2003, **51**, p 4791–4801

29. D. Allehaux and F. Marie, Mechanical and Corrosion Behavior of the 2139 Aluminum-Copper-Alloy Welded by the Friction Stir Welding Using the Bobbin Tool Technique, *Mater. Sci. Forum*, 2006, **519–521**, p 1131–1138

30. Y.S. Sato, S. Hwan, C. Park, and H. Kokawa, Microstructural Factors Governing Hardness in Friction-Stir Welds of Solid-Solution-Hardened Al Alloys, *Metall. Mater. Trans. A*, 2001, **32A**, p 3033–3042

31. L. Fratini, G. Buffa, and D. Palmeri, Using a Neural Network for Predicting the Average Grain-Size in Friction Stir Welding Processes, *Comput. Struct.*, 2009, **87**, p 1166–1174

32. "Military Standard for Welding of Aluminum Alloy Armor," MIL-STD-1946A, U.S. Department of Defense, Washington DC, January 1990

33. A. Wenzel and J.M. Hennessey, Analysis and Measurements of the Response of Armor Plates to Land Mine Attacks, *Proceedings of the Army Symposium on Solid Mechanics*, Warren, Michigan, July 1972, p 114–128